Published paper
Black, L., Garbev, K. and Stumm, A. (2009) *Structure, bonding and morphology of hydrothermally- synthesised xonotlite.* Advances in Applied Ceramics, 108 (3). pp. 137-144.

http://dx.doi.org/10.1179/174367608X353638

Structure, Bonding and Morphology of Hydrothermally-Synthesised Xonotlite

Leon Black[a,b], Krassimir Garbev[b], Andreas Stumm[b,c]*

a. University of Leeds, School of Civil Engineering, Leeds, LS2 9JT, UK.

b. Forschungszentrum Karlsruhe GmbH (ITC-TAB), Hermann-von-Helmholtz-Platz 1, 76344 Eggenstein-Leopoldshafen, Germany.

c. Xella Technologie- und Forschungsgesellschaft mbH, Hohes Steinfeld 1, D-14797, Kloster Lehnin, Germany.

Abstract

We have systematically investigated the role of synthesis conditions upon the structure and morphology of xonotlite. Starting with a mechanochemically-prepared, semi-crystalline phase with Ca:Si = 1, we have prepared a series of xonotlite samples hydrothermally, at temperatures between 200 and 250°C. Analysis in each case was by x-ray photoelectron spectroscopy (XPS), environmental scanning electron microscopy (ESEM) and x-ray diffraction (XRD). There was increased silicate polymerisation with both increased synthesis temperature and duration of synthesis. Concerning crystal morphology, there was an increase in crystal size with increasing temperature, but this led to some crystal damage. Longer hydrothermal treatment however led to more perfect crystal morphologies.

* Corresponding author.

Email: l.black@leeds.ac.uk

Keywords

Xonotlite, hydrothermal treatment, silicate polymerisation, structure, synthesis, XPS

Introduction

Xonotlite, $Ca_6Si_6O_{17}(OH)$ (or C_6S_6H[†] in cement chemistry notation) is a crystalline, calcium silicate hydrate. First discovered by Rammelsberg in 1866, the most prominent occurrences are Tetela de Xonotla (Mexico), (whence the mineral's name), Crestmore (USA), Franklin (USA), Scwat Hill (Ireland) and Wessels mine (RSA). The chemical composition of most natural xonotlite samples does not differ substantially from the ideal formula, with traces of Fe, Mn and Na occasionally being incorporated. Qian *et al.* [1] showed that significant Mg substitution may occur, until $Ca_{3.58}Mg_{2.41}Si_{6.04}O_{17}(OH)_2$ is obtained.

However, mining cannot be justified economically, and applications have concentrated on the use of synthetic xonotlite, where of purity and mineralogy can be controlled. Much of the literature concerning hydrothermally treated calcium silicate hydrates is concerned with the effects of various synthesis parameters on the formation of tobermorite or phases with lower Ca/Si ratios, for example [2-3456]. However, there is still interest in the formation of synthetic xonotlite for a number of applications. Xonotlite is an important constituent in thermally-cured, cement-based materials [7,8]. It has also been used for its thermo-insulating properties [910,1112], and its use as a filler material has been reported many times, e.g. to improve the flexural strength of cement matrices [13], or as a filler in organic polymers in either moulded materials [14] or brake linings [15]. With ever more pressure to produce more environmentally benign materials, there ha been

[†] We have used accepted cement chemistry nomenclature, whereby C, S and H indicate the oxides of calcium, silicon and hydrogen respectively

further work investigating the incorporation of magnesium into xonotlite, and hydrothermally synthesised xonotlite and magnesium-substituted xonotlite monoliths have been shown to possess considerable compressive strengths and dimensional stabilities [16].

The structure of xonotlite, and the conditions under which it may be formed is also of interest to the oil and gas industry, where oil well cements may encounter temperatures and pressures of up to 200ºC and 1000 bar when present between the steel well casing and the surrounding rock [17]. High temperatures together with either high or ambient pressures may also be present in long-term nuclear storage facilities, leading to interest in xonotlite formation and stability from this perspective also [18,19].

Xonotlite's structure was initially described by Mamedov and Belov [20] and subsequently by Kudoh and Takeuchi [21]. It comprises double silicate chains [Si_6O_{17}], so called Dreierdoppelketten [22], linked via undulating sheets of edge sharing Ca-polyhedra stacked along the *c* direction. There are two types of Ca-polyhedra, 1/3 of which are 6-fold coordinated and 2/3 being 7-fold coordinated [21]. Adjacent Ca-polyhedral sheets are about 7 Å apart along the c axis corresponding to the (002) reflection in the powder diffraction pattern. Two different translation mechanisms, concerning the arrangement of the double chains relative to one another, give rise to four simple polytypes.

Xonotlite forms readily under hydrothermal conditions above 180°C [2] and is the predominant stable phase over the range 180-300°. At lower temperatures, 11 Å tobermorite is almost always present, with an 11 Å tobermorite-xonotlite-transition temperature of about 140°C [2- 3 4], although the stability of 11 Å tobermorite increases with its aluminium content [5]. Kinetic

studies confirm that tobermorite is an intermediate in the formation under hydrothermal conditions of xonotlite from calcium silicate hydrate. Shaw *et al.* [5] proposed that under hydrothermal conditions, C-S-H was converted initially to a defect tobermorite structure and then to either tobermorite or xonotlite via ordering of the octahedral CaO sheets. Hydrothermal treatment of lime-silica-quartz mixtures with Ca/Si ratios of 0.8 at temperatures between 120 and 180ºC for up to 20 hours produced only tobermorite [6]. However, Chan *et al*. did observe the formation of xonotlite-tobermorite mixtures from the same samples treated at 180ºC for 20 hours or longer, and just xonotlite when the Ca/Si ratio was 1 after treatment beyond 20 hours at 180ºC [6]. Kalousek *et al*. [9] state that the conversion of tobermorite to xonotlite is topotactic, i.e. occurs with no change in particle morphology, and for this reason synthetic xonotlites are often found to be slightly calcium deficient, with charge balancing being achieved by Si-OH groups.

Under hydrothermal conditions with Ca/Si ratios of 0.5 to 1.0, xonotlite-gyrolite mixtures coexist over the temperature range 200-300°C, [19,23,24] whilst xonotlite and truscottite are stable above 300°C [25]. Upon dehydration, at 780-835°C, xonotlite is converted topotactically to β-$CaSiO_3$ (wollastonite) [5], possibly via an intermediate structure occurring at about 735°C [26].

In this study we hope to show how the synthesis conditions of hydrothermally synthesised xonotlite influence the resultant structure, in particular the extent of silicate polymerisation and crystal morphology. Starting with a semi crystalline C-S-H phase (C-S-H(I) with Ca/Si=1.00), we have prepared xonotlite hydrothermally at three different temperatures (200, 220 and 250°C) with subsequent analysis by XRD, XPS and ESEM.

Experimental

Sample Preparation

Semi-Crystalline C-S-H I (Ca/Si = 1)

The precursor for the synthesis of the crystalline xonotlite was a C-S-H gel with Ca/Si = 1. This phase was synthesised according to the procedure of Saito *et al.* [27]. A freshly-prepared, stoichiometric mixture of CaO (from reagent grade $CaCO_3$ (Merck) treated at ca. 1000°C), highly dispersed SiO_2 (Aerosil) and doubly distilled water (boiled so as to remove CO_2) (w/s = 4) was ground for 12 hours in an agate ball mill. The mill was loaded under nitrogen, in a glove box, to prevent reaction with atmospheric carbon dioxide, so called carbonation. After mechanochemical treatment, the mill was emptied and the sample dried at 60°C in the glove box.

Synthetic Xonotlite

The crystalline xonotlite samples were prepared via hydrothermal treatment of the gel phase described above. The C-S-H gel was treated hydrothermally for 1 week at 200, 220 or 250°C in PTFE inserts within steel autoclaves. An additional sample was synthesised at 220°C for 2 weeks. Hydrothermal treatment either at lower temperatures or for shorter than 1 week were investigated, but these were found to yield 11 Å tobermorite over xonotlite, which is known to be metastable under such conditions [4], indeed in many other studies into the formation and stability of xonotlite, tobermorite-xonotlite mixtures have been the early stage or low temperature reaction products [2-5]. After hydrothermal treatment, the samples were washed with ethanol and dried at 60°C in a drying cabinet. The presence of tobermorite after such long periods contradicts the findings of Chan *et al*. who found xonotlite after hydrothermal treatment beyond 20 hours [2]. However, they used a w/s ratio of 20, aiding silicate dissolution and hence xonotlite formation. Our use of a much lower w/s ratio necessitated a longer synthesis time.

XRD

X-ray diffraction was performed in reflection mode using a D8 Advance diffractometer (Bruker-

AXS) equipped with a CuKα anode and a silicon solid-state energy dispersive detector. Measurements were performed over the 2θ-range 5-140°, with a 0.02°2θ step size and 15s/step. A set of variable slits (VDS) were used to maintain an illuminated sample length of 20 mm.

XPS

Each sample was analysed as received, with the powders being pressed onto adhesive-backed copper tape before introduction into the vacuum chamber. Analysis was performed using a VG Escascope fitted with a MgK_{α} (hν=1253.6 eV) X-ray source operating at 260 W (13 kV, 20 mA). After an initial wide spectrum, regional spectra were recorded with a 30 eV pass energy for the important elemental lines, (Si 2p, Si 2s, Ca 2p, O 1s and C 1s).

Data were extracted from the spectra via peak fitting using XPSPeak software (available by download from: http://www.phy.cuhk.edu.hk/~surface/). A Shirley background and an 80:20 Gaussian:Lorentzian peak shape was assumed in all cases. Spectra were corrected for charging effects against the adventitious carbon peak at 284.8 eV.

ESEM

Sample morphology was investigated using a Philips XL30-FEG Environmental Scanning Electron Microscope (Philips, Eindhoven, Netherlands). The images were obtained using a gaseous secondary electron detector with water vapour as the imaging gas. Typical operating conditions were a water vapour partial pressure of 1.0 mBar and 10 kV accelerating voltage, although slight variations were occasionally used to optimise image quality. Powder samples were prepared by sprinkling the powders onto adhesive-backed carbon foils, which were then fixed to the sample holders and introduced into the microscope.

Results and Discussion

XRD

The phases identified in the X-ray powder diffraction patterns of the various samples are shown in Figure 1. The mechanochemically prepared sample comprises predominately C-S-H (I) (ICDD No. 34-0002) and thus resembles the poorly-crystalline product formed upon hydration of Portland cement. The powder diffraction pattern of C-S-H (I) itself closely resembles that of 11 Å tobermorite [28,29]. This is illustrated by the additional diffraction patterns shown in Figure 1, i.e. a mechanochemically synthesised C-S-H phase with C/S = 1 prior to any hydrothermal treatment (MCT C/S=1.0 RT) and 11 Å tobermorite prepared by hydrothermal treatment at 170°C for 5 days of a mechanochemically synthesised C-S-H with C/S = 5/6 (MCT C/S=5/6 170ºC 5d). The hydrothermally treated samples all comprise primarily xonotlite, with traces of calcite, although the sample prepared at 200°C also shows a small quantity of 11 Å tobermorite. The diffraction patterns are sharper than those often published for synthetic xonotlite, for example [12,16], which is in support of Hamilton and Hall's statement that synthetic xonotlite often exhibits a lower degree of crystallinity than natural samples [11]. However, the hydrothermal treatment times were considerably longer in our experiments than in many previous studies. As mentioned elsewhere in this manuscript, the lower w/s ratios used in our study led to reduced silicate dissolution, and therefore necessitated longer hydrothermal treatment. This subsequently appeared to have a positive influence on the degree of crystallinity.

There is strong evidence of preferred xonotlite orientation in the different samples. The strongest peak for xonotlite is 320 according to ICDD 23-0125 or 2-20(120) according to Kudoh and Takeuchi [21] (i.e. at 3.08Å). This peak dominates the powder diffraction pattern of the sample

prepared at 200°C, indicating a relatively low degree of preferred orientation. With increasing temperature, the peaks 00l and h0l dominate the diffraction patterns, indicating preferred orientation. For example, the strongest peaks in the powder pattern of the sample prepared at 250°C are –402(2.7 Å), 202(3.23 Å) and 001(7 Å) (indexed according ICDD No. 23-0125). It should be noted however that increasing synthesis temperatures led to longer, thinner crystals (see below), and this may be the cause of the increased preferential orientation described above.

Increased synthesis temperature also led to improved resolution of the peak 026(1-26) according to [21] at 1.957 Å, visible as a shoulder to the left of the strong peak at 1.947 Å (322), and the peak at 3.2 Å (022(1-22) according to [21]). Generally, the sample synthesised at 200°C showed the broadest reflections, in agreement with the findings of others [5,9,16], implying the smallest coherent scattering domains. Trends in the breadth of the other peaks were dependent upon the reflection of interest, and may be due to the formation of different polytypes at different temperatures. However, at present this is uncertain and will form part of a future study.

XPS

X-ray photoelectron spectroscopy (XPS) is a technique well suited, but little utilised, for the study of structural changes in mineral systems. We have shown how XPS may be used to investigate the structures of crystalline calcium silicates [30] and calcium silicate hydrates [31-34], relating spectral features to structural changes. Binding energies and peak widths (in particular the silicon 2p and 2s lines) provide information as to the extent of silicate polymerisation and the degree of structural disorder. Phases may additionally be described in terms of the energy separation between the Ca 2p and Si 2p peaks. This approach was used by Regourd *et al.* [35] and Thomassin *et al.* [36] when investigating the hydration of tricalcium

silicate and dicalcium silicate respectively, and more recently by ourselves when investigating the natural aging of both of these phases [30]. Additionally, structural information can also be gleaned from examination of the O 1s spectra, in particular the energy separation and peak intensities of signals ascribed to bridging and non-bridging oxygen species [33].

Earlier studies posed an interesting question. If increased polymerisation can be followed by changes in photoelectron spectra, how sensitive is XPS to differing degrees of crystallinity?

Various relevant spectral data are presented in Table 1, and for increased clarity in figures 2-4. Also, for comparison, we present the data for mechanochemically synthesised C-S-H with C/S = 1 and a pure 11 Å tobermorite sample, with a Ca/Si ratio = 0.83, prepared hydrothermally at 180°C for 5 days.

The mechanochemically prepared sample had a Si 2p binding energy of 101.82 eV. Aside from our studies [30-34], we have been unable to find other XPS studies of pure C-S-H phases, but McWhinney *et al.* [37] and Mollah *et al.* [38] reported Si 2p binding energies of 101.5 and 102 eV for hydrated OPC respectively[‡]. Similarly, Thomassin *et al.* observed a Ca-Si energy separation of 244.9 eV after hydration of dicalcium silicate for 4 days [36], whilst Regourd *et al.*

[‡] Note: there is some uncertainty over the precise binding energy of the C 1s signal from adventitious carbon, used to correct for sample charging. We have used a value of 284.8 eV, but values between 284.6 and 285 eV may be found in the literature. Accordingly, when quoting binding energies from the literature, we have re-calculated the binding energies against an adventitious carbon signal at 284.8eV. We have refrained from quoting data where the extent of charge correction has not been stated.

reported a separation of 245.1 eV after hydration of tricalcium silicate for 4 hours [35]. This compares with a value of 245.19 eV for our mechanochemically prepared sample. Thus, we may say that, on the basis of the degree of silicate polymerisation, the semi-crystalline C-S-H phase is similar to that found in hydrated ordinary Portland cement. This is confirmed by recent Raman analysis of mechanochemically synthesised C-S-H phases, which were found to possess tobermorite-like structures [39].

There are marked changes in the spectra upon hydrothermal treatment, i.e. upon crystallisation of xonotlite, most noticeably in the Si 2p spectra, (Figure 2). Hydrothermal treatment leads to an increase in Si 2p binding energies, implying a higher degree of silicate polymerisation [30-34,38-41]. Similarly, Chen *et al.* [42] observed a decrease in Ti 2p binding energies of gadolinium titanates upon their amorphization, attributed to an increase in the covalent nature of the amorphous phases over the crystalline ones. Comparing the results from the three samples synthesised for 1 week, there is an increase in Si 2p binding energy with increasing synthesis temperature, indicating increased silicate polymerisation, although, as with the XRD data, the effect diminishes with ever increasing synthesis temperature.

Hydrothermal treatment also leads to sharper Si 2p peaks, the peaks becoming ever sharper with increasing synthesis temperature. If we consider that shifts in binding energies reflect changes in the electronic environment of an element, then sharper peaks indicate the presence of fewer environments, i.e. a more ordered structure. Thus, we may assume the semi-crystalline phase to posses a disordered structure, becoming more ordered upon crystallisation of xonotlite, and increasingly so with higher synthesis temperatures. This, together with the binding energy and XRD data may indicate that the structure is becoming more ordered. This is not unexpected, and

has been seen in the XRD results of many other studies, for example [2,6,16]. Kalousek *et al*. postulated that higher temperatures should accelerate the topotactic tobermorite-xonotlite recrystallisation, therefore leading to more rapid improvements in xonotlite crystallinity [9].

In Table 1 we also report the Si 2s binding energies and peak widths. It is more common to report the Si 2p lines, these being sharper and more intense than the Si 2s lines. However, other authors have reported problems measuring the former when using aluminium K_α X-ray sources [40,43]. Therefore, to enable ready comparisons between our results and others, we measured both sets of lines. Trends were equally evident in both sets of lines.

As for the silicon spectra (Si 2p and Si 2s), there is a significant increase in Ca 2p binding energies upon hydrothermal treatment. However, in this instance there is no further dependency upon synthesis temperature or duration. We suppose that crystallisation leads to shorter Ca-O bonds and thus slightly higher Ca 2p binding energies. We observed a slight relationship between structure and Ca $2p_{3/2}$ binding energies for numerous crystalline C-S-H phases [31]. However, this was related to changes in calcium coordination number rather than the extent of polymerisation. We did not see a dependency upon C/S ratio when examining a series of mechanochemically synthesised C-S-H samples [34]. Thus we can infer changes in the strength of bonding upon hydrothermal treatment, but no significant changes in bonding dependent upon synthesis conditions.

As mentioned above, the energy separation between the Ca $2p_{3/2}$ and Si 2p peaks has previously been used to assess the extent of silicate polymerisation [30,34,35,36], there being a decrease in energy separation with increasing polymerisation. This approach has the advantage of negating

errors due to charge correction, but does not allow comparisons between phases that are too dissimilar. For instance, calcium and magnesium silicates may not be compared. Accordingly, the data shown in Table 1 and Figure 3 illustrate how both increased synthesis temperature and duration lead to increased silicate polymerisation.

The final method used to assess the extent of polymerisation is the separation of the bridging and non-bridging components of the O 1s spectra. This has often been used for the examination of glass samples. Mekki and Salim observed a decrease in peak separation when the electronic environments of the bridging and non-bridging oxygen atoms were more similar [44]. In their case this was a result of the presence of different metals in silicate glasses. However, we have recently found that the peak separation may also be related to the extent of silicate polymerisation [33], whereby for a given anion type, the separation decreases with increasing polymerisation. Thus, as seen in Table 1 and Figure 4, assuming that all of the phases are inosilicates, i.e. chain silicates, the phases are increasingly polymerised with increasing synthesis temperature.

Finally, as mentioned above, in Table 1 and figures 2 – 4 we show the equivalent recorded data from an 11 Å tobermorite sample, with a Ca/Si ratio = 0.83, prepared hydrothermally at 180°C for 5 days. We have stated earlier that xonotlite syntheses attempted at lower temperatures or for periods of less than 1 week yielded 11 Å tobermorite. As mentioned earlier, it is well-known that 11 Å tobermorite is an intermediary in the formation of xonotlite [2,9]. From the data in Table 1, it is clear that, on the basis of the extent of polymerisation, 11 Å tobermorite is an intermediate phase between the semi-crystalline C-S-H gel and crystalline xonotlite. Note that the Ca $2p_{3/2}$ binding energy is a little lower than the other samples, but this is a result of the increased calcium

coordination number in 11 Å tobermorite compared to xonotlite.

ESEM

Figures 5 to 9 show ESEM images of the various samples. The mechanochemically prepared sample shows no distinct features, appearing simply as a poorly-defined mass (Figure 5). Hydrothermal treatment led to the formation of needle or lath-like xonotlite crystals typical of xonotlite [12,16,17].

Samples prepared at 200°C were typically 10-20 μm long with flat ends (Figure 6). Hydrothermal treatment at increasing temperatures led to the formation of longer and thinner crystals. At 220°C the crystals were approximately 20-30 μm long, but with feathered, rather than flat, ends (Figure 7). We presume this feathering to be a result of calcium dissolution from between the silicate chains. This proceeds from the ends of the crystals, where the calcium sheets are in contact with the water in the autoclave. Synthesis at 250°C led to crystals approximately 30-40 μm long (Figure 8). However, these crystals were much thinner than those formed at lower temperatures. We assume that at these higher temperatures there had been more pronounced loss of calcium leading to splitting of the crystals along their c-axis. Similar behaviour and similar crystal morphologies have been observed upon exposing xonotlite to ammonium nitrate, a calcium chelating agent [45], also associated with the loss of the polyhedral calcium sheets.

Increased duration of hydrothermal treatment did not lead to the synthesis of longer crystals. Crystals synthesised at 220°C for 1 or 2 weeks were still approximately 20-30 μm long, but without the feathering as seen after 1 week (Figure 9). Rather, the crystals had a similar appearance to those formed after 1 week at 200°C, only longer.

As with the XRD and XPS data, hydrothermal treatment of a mechanochemically synthesised C-S-H sample with a tobermorite-like structure, leads to significant structural changes, with xonotlite being formed at 200°C. Hydrothermal treatment at higher temperatures led to only slight further changes. The xonotlite crystals formed in this study were considerable larger than hose formed in many other investigations. Takahashi *et al*. [12] synthesised 10 µm long xonotlite crystals after hydrothermal treatment at 200°C for 8 hours with a w/s ratio of 20. Under the same conditions, but in the presence of pulp fibres, the crystals were just 3 µm long and 0.2 µm wide. Similarly, Mitsuda *et al*. [8] observed the formation of xonotlite fibres considerably smaller than 10 µm after 64 hours at 180°C with a w/s ratio of 0.70. This agrees closely with Milestone and Ghanbari Ahari [16], who also saw sub 10 µm crystals of xonotlite after 24 hours under autogeneous steam pressure at 200-250°C with w/s ratios of 0.44 to 0.94. Based upon comparisons between our results and these three articles, it appears to be the duration of treatment which has the greatest influence upon crystallite size, rather than temperature or w/s ratio.

Conclusions

- **What is the significance of the present work?**
- **What are the main differences between the present work and that reported by others?**
- **The effects of processing parameters on the synthesis are summarised. However, the relevant mechanisms/reasons are not given.**

We have synthesised xonotlite hydrothermally from a C-S-H gel with Ca/Si = 1 and w/s = 4, with analysis by X-ray diffraction, X-ray photoelectron spectroscopy and environmental scanning electron microscopy. To ensure pure xonotlite, i.e. free from tobermorite, it was necessary to

synthesise the samples at 220°C for one week, although at 200°C only traces of xonotlite remained. This contradicts Chan *et al*. [2] who obtained xonotlite after just 20 hours of hydrothermal treatment. However, since silicate dissolution is a key step in the formation of xonotlite, our use of a much lower w/s ratio (4 as opposed to 20) necessitated a longer synthesis period.

Control of the synthesis parameters, i.e. temperature and duration of hydrothermal treatment, enabled control of the extent of polymerisation and crystal size. The findings are summarised below:

- In agreement with many other studies, increased synthesis temperature led to increased silicate polymerisation (seen via the increased Si 2p binding energies) and increased structural ordering (seen via the sharpening of the Si 2p photoelectron peaks).
- Increased synthesis temperature led to larger crystals, but the crystals also appeared to have split along their length.
- Increasing the duration of hydrothermal treatment from one to two weeks led to increased silicate polymerisation.
- Longer hydrothermal treatment did not lead to the formation of larger crystals, but did lead to more perfect crystal morphologies.

Acknowledgements

Our sincerest thanks are given to Dr Keith Hallam and Professor Geoff Allen at the University of Bristol Interface Analysis Centre, UK, for, respectively, their technical assistance with and access to the x-ray photoelectron spectrometer.

Figures

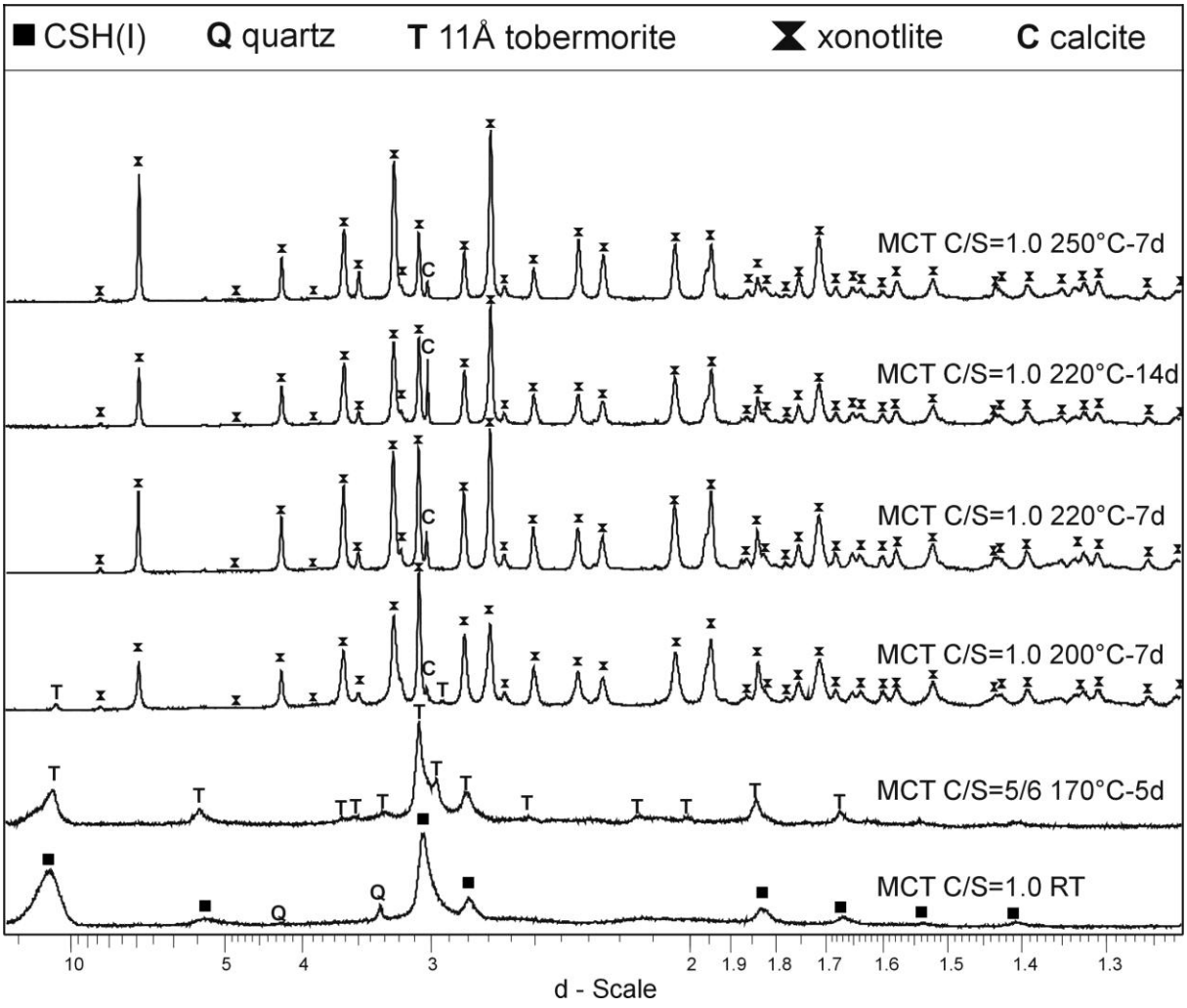

Figure 1

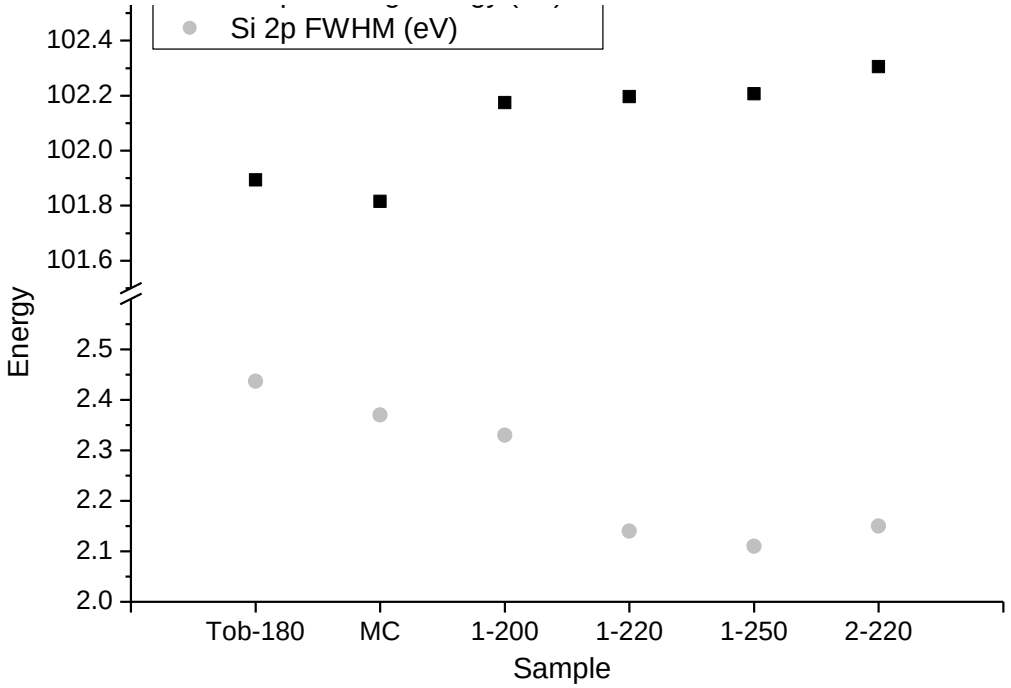
Si 2p FWHM (eV)
102.4
102.2
102.0
101.8
101.6
2.5
2.4
2.3
2.2
2.1
2.0
Energy
Tob-180
MC
1-200
1-220
1-250
2-220
Sample

Figure 2

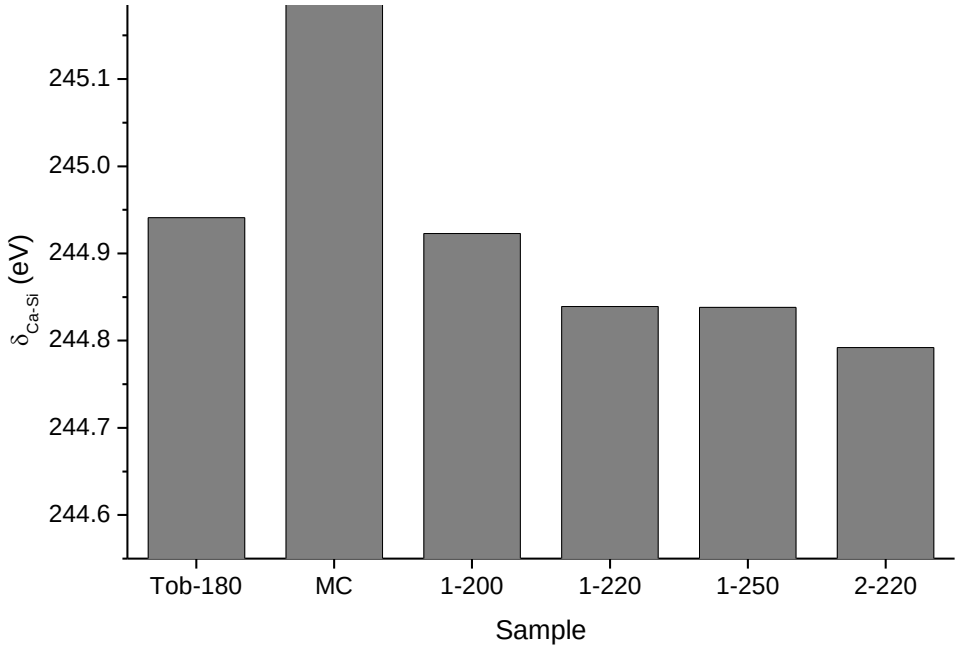
245.1
245.0
244.9
244.8
244.7
244.6
δCa-Si (eV)
Tob-180
MC
1-200
1-220
1-250
2-220
Sample

Figure 3

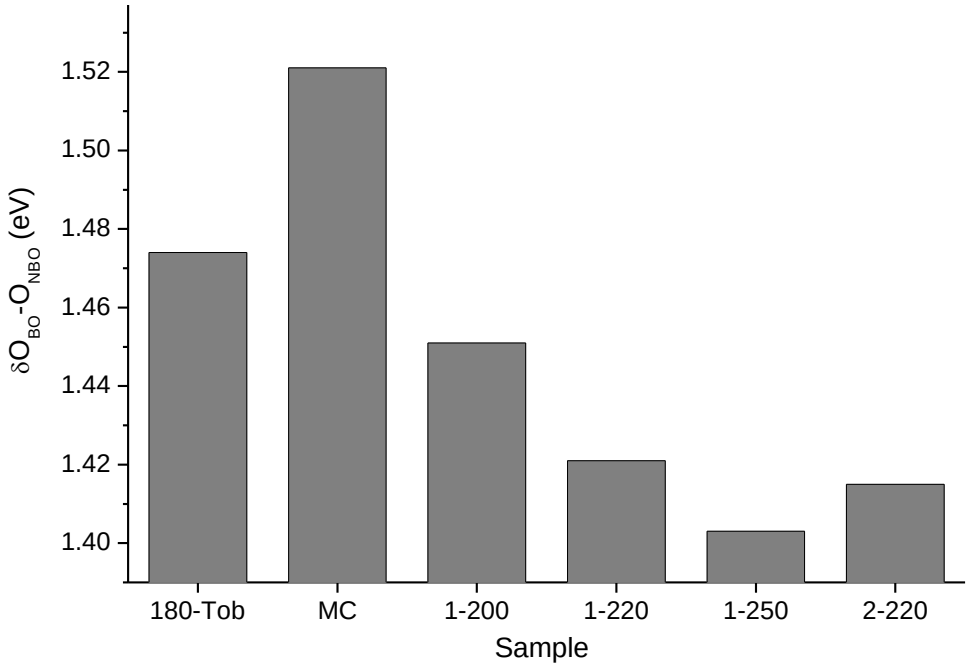
1.52
1.50
1.48
1.46
1.44
1.42
1.40
δO_BO-O_NBO (eV)
180-Tob
MC
1-200
1-220
1-250
2-220
Sample

Figure 4

Figure 5

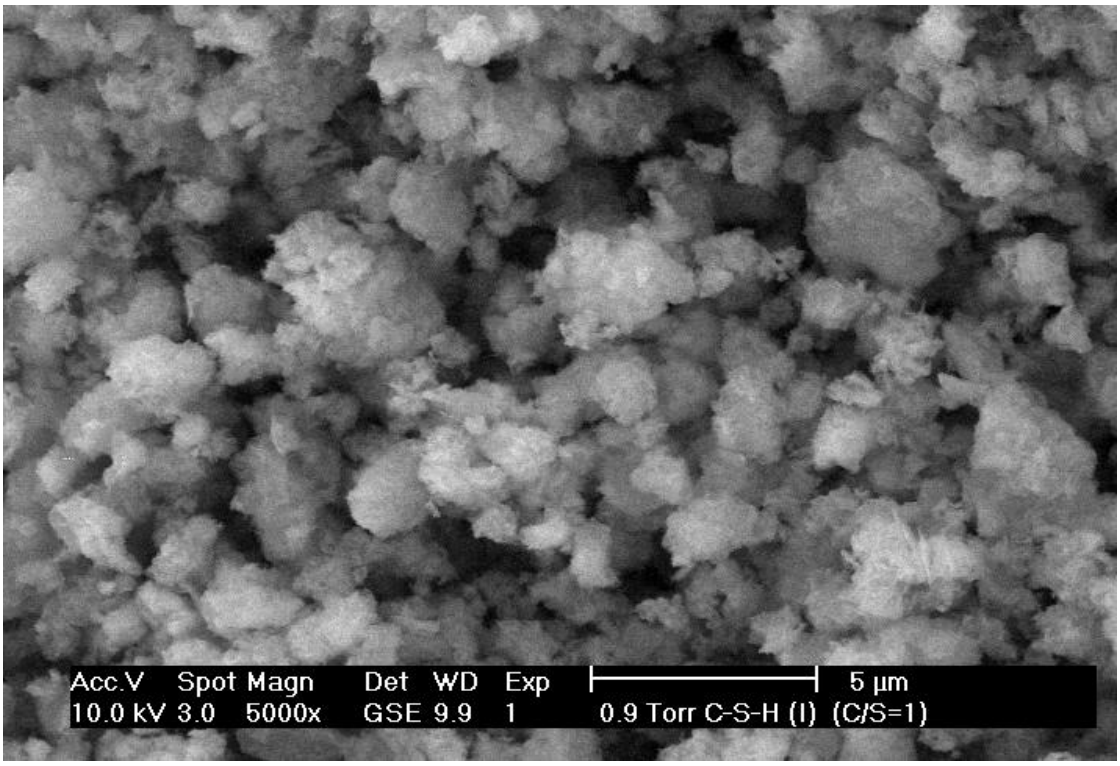
Acc.V Spot Magn Det WD Exp 5 µm
10.0 kV 3.0 5000x GSE 9.9 1 0.9 Torr C-S-H (I) (C/S=1)

Figure 6

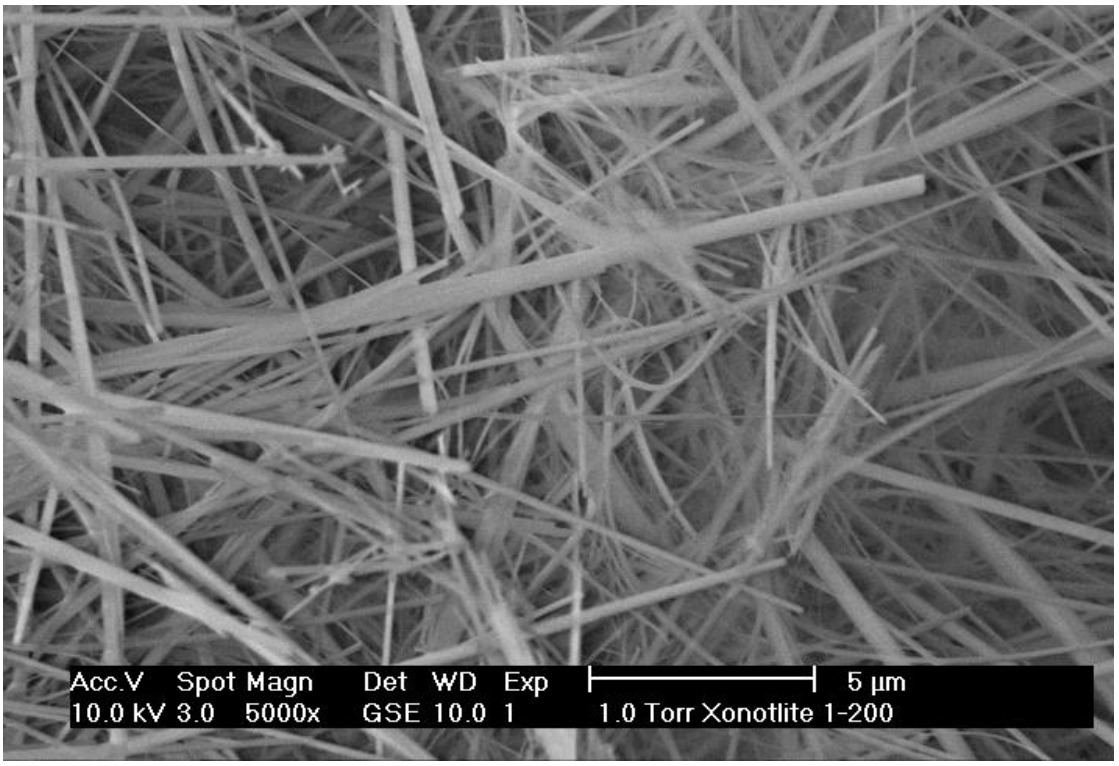
Acc.V Spot Magn Det WD Exp 5 µm
10.0 kV 3.0 5000x GSE 10.0 1 1.0 Torr Xonotlite 1-200

Figure 7

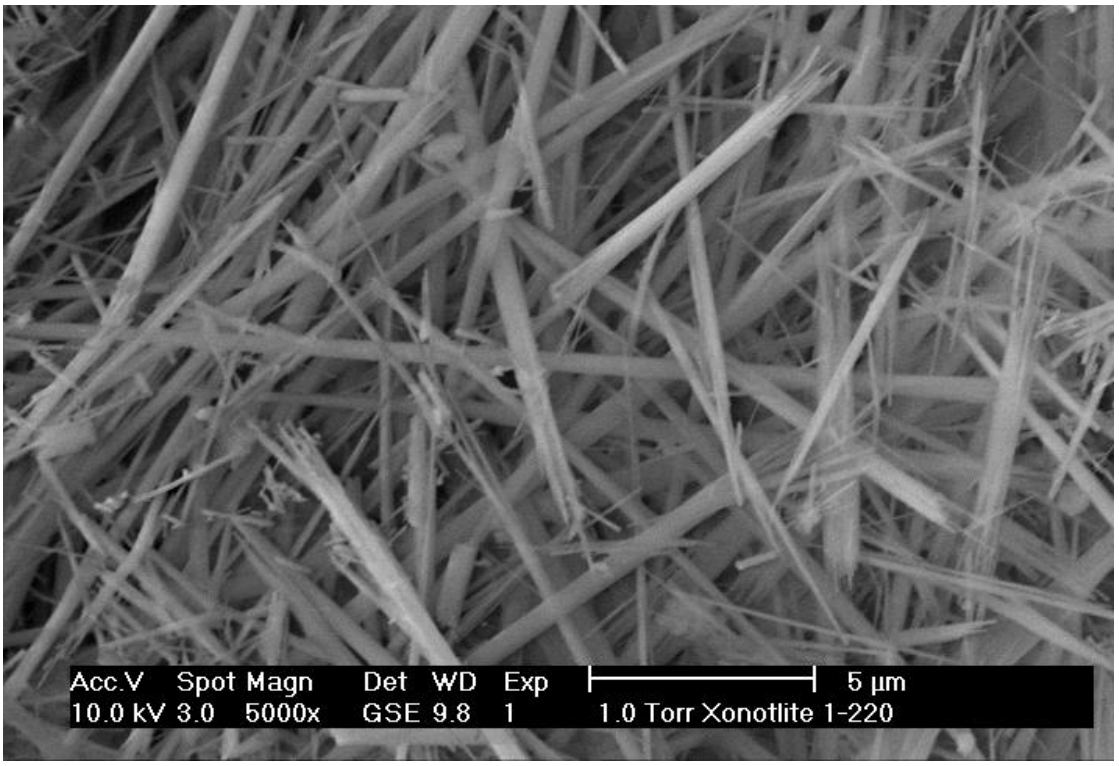
Acc.V Spot Magn Det WD Exp 5 µm
10.0 kV 3.0 5000x GSE 9.8 1 1.0 Torr Xonotlite 1-220

Figure 8

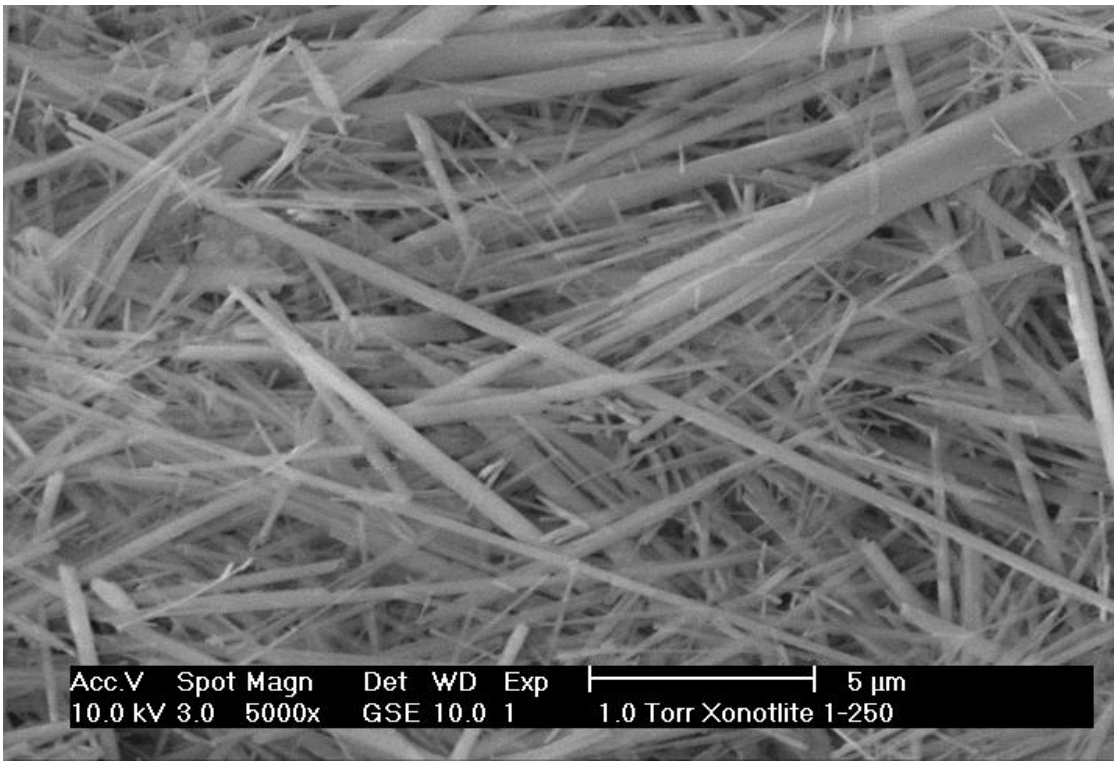
Acc.V Spot Magn Det WD Exp 5 µm
10.0 kV 3.0 5000x GSE 10.0 1 1.0 Torr Xonotlite 1-250

Figure 9

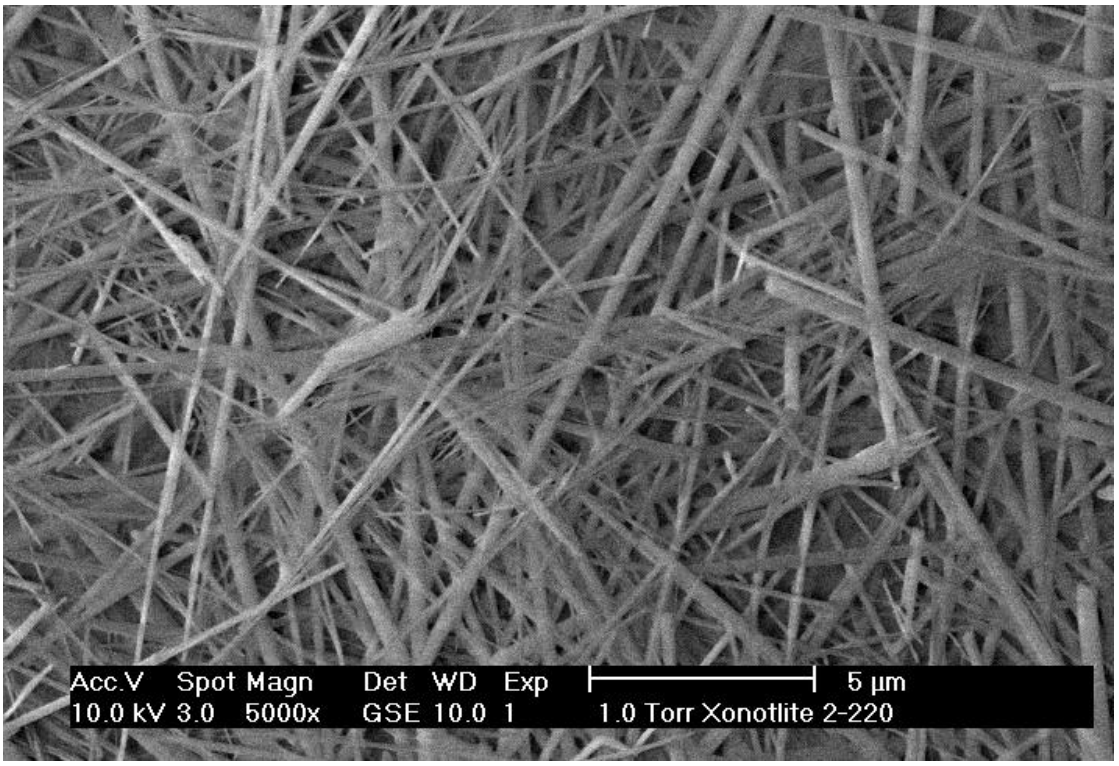
Acc.V Spot Magn Det WD Exp 5 µm
10.0 kV 3.0 5000x GSE 10.0 1 1.0 Torr Xonotlite 2-220

Tables

Table 1: Various XPS spectral data from the different phases analysed.

Energy (eV)	Tob-180	MC	1-200	1-220	1-250	2-220
Si 2p						
Binding Energy	101.89	101.82	102.18	102.20	102.21	102.31
FWHM	2.44	2.37	2.33	2.14	2.11	2.15
Si 2s						
Binding Energy	152.92	152.87	153.21	153.21	153.23	153.40
FWHM	3.33	3.22	3.16	2.86	3.00	2.94
Ca $2p_{3/2}$						
Binding Energy	346.83	347.01	347.10	347.04	347.04	347.10
FWHM	2.03	2.13	1.88	1.81	1.75	1.83
$\delta_{Ca\text{-}Si}$	244.94	245.19	244.92	244.84	244.84	244.79
$\delta_{BO\text{-}NBO}$	1.474	1.521	1.451	1.421	1.403	1.415

Figure Captions

Figure 1. X-ray powder diffraction patterns of the various samples. The reflections of the mechanochemically prepared sample with C/S=1.0 shows a close similarity to those of C-S-H(I) and 11 Å tobermorite.

Figure 2: Changes in Si 2p binding energy and FWHM depending upon synthesis conditions.

Figure 3: Changes in δCa-Si, (the energy separation between the Ca 2p3/2 and Si 2p peaks) depending upon synthesis conditions.

Figure 4: Changes in δBO-NBO, (the energy separation between bridging and non-bridging components of the O 1s signals), depending upon synthesis conditions.

Figure 5: Mechanochemically prepared C-S-H, Ca/Si = 1.00

Figure 6: Xonotlite prepared hydrothermally at 200°C for one week.

Figure 7: Xonotlite prepared hydrothermally at 220°C for one week.

Figure 8: Xonotlite prepared hydrothermally at 250°C for one week.

Figure 9: Xonotlite prepared hydrothermally at 220°C for two weeks.

References

1 G. R. Qian, G. L. Xu, H. Y. Li, A. M. Li, "Mg- Xonotlite and its Coexisting Phases". *Cem. Concr. Res.*, 27[3] 315-320 (1997).

2 C. F. Chan, M. Sakiyama, T. Mitsuda, „Kinetics of the CaO – Quartz – H_2O Reaction at 120º to 180ºC in Suspensions". *Cem. Conc. Res.*, 8 1-6 (1978).

3 R. Gabrovsek, B. Kurbus, D. Mueller, W. Weiker, "Tobermorite Formation in the System CaO-C_3S–SiO_2–Al_2O_3–NaOH–H_2O Under Hydrothermal Conditions". *Cem. Concr. Res.*, 23[2] 321–328 (1993).

4 S. A. S. El-Hemaly, T. Mitsuda, H. F. W. Taylor, "Synthesis of Normal and Anomalous Tobermorite". *Cem. Concr. Res.*, 7 429–432 (1977).

5 S. Shaw, S. M. Clark, C. M. B. Henderson, "Hydrothermal Formation of the Calcium Silicate Hydrates Tobermorite ($Ca_5Si_6O_{16}(OH)_2.4H_2O$) and Xonotlite ($Ca_6Si_6O_{17}(OH)_2$): an in-situ Synchrotron Study", *Chem Geol* 167 129–140 (2000).

6 C. F. Chan, T. Mitsuda, "Formation of 11 Å Tobermorite from Mixtures of Lime and Colloidal Silica with Quartz", *Cem. Conc. Res.*, 8 135-138 (1978).

7 A. Feylessoufi, M. Crespin, P. Dion, F. Bergaya, H. Van Damme, P. Richard, "Controlled Rate Thermal Treatment of Reactive Powder Concretes", *Advn. Cem. Bas. Mat.*, 6 21-27 (1997).

8 T. Mitsuda, K. Sasaki, H. Ishida "Phase Evolution during Autoclaving Process of Aerated Concrete", *J. Am. Ceram. Soc*, 75(7) (1992) 1858-1863.

9 G. L. Kalousek, T. Mitsuda, H. F. W. Taylor, "Xonotlite: Cell Parameters, Thermogravimetry and Analytical Electron Microscopy". *Cem. Concr. Res*., 7[3], 305-312 (1977).

10 Q. Zheng, W. Wang, "Calcium Silicate Based High Efficiency Thermal Insulation", *Brit. Ceram. Trans.*, 99[4], 187-190. (2000).

11 A. Hamilton, C. Hall, "Physicochemical Characterization of a Hydrated Calcium Silicate Board Material", *Journal of Building Physics*, 29 9-19 (2005), DOI: 10.1177/1744259105053280.

12 K. Takahashi, N. Yamasaki, K. Mishima, K. Matsuyama, H. Tomokage, "Coating of pulp fiber with xonotlite under hydrothermal conditions", *J. Mater. Sci. Let*., 21, 1521-1523, (2002).

13 N. M. P. Low, J. J. Beaudoin, "Mechanical Properties and Microstructure of Cement Binders Reinforced with Synthesized Xonotlite Micro-Fibres", *Cem. Concr. Res.*, 23, 1016-1028, (1993).

14 H. Tanaka, Y. Asano, K. Watanabe, H. Uchimura, "Xonotlite-Reinforced Organic Polymer Composition as Molding Material for Automobile Parts, Electric and Electronic Parts, Civil Engineering Equipment Components, Precision Machinery Components, and the Like", US Patent. No. 5,623,013. (1997).

15 O. Anton, A. Eckert, A. Eckert, "Asbestos-Free Brake Lining Comprising Phenolic Resin and Usual Fillers and in Addition an Amount of a Synthetic Hydrated Calcium Silicate Particle of Xonotlite", US Patent. No. 4,994,506. (1991).

16 N. B. Milestone, K. Ghanbari Ahari, "Hydrothermal processing of xonotlite based compositions", *Adv. App. Ceram.*, 106(6) 302-308 (2007).

17 F. Méducin, B. Bresson, N. Lequeux, M.-N. de Noirfontaine, H. Zanni, "Calcium Silicate Hydrates Investigated by Solid-State High Resolution ^{1}H and ^{29}Si Nuclear Magnetic Resonance", *Cem. Conc. Res.*, 37 631–638 (2007).

18 F.P. Glasser, S.-Y. Hong, "Thermal treatment of C–S–H gel at 1 bar H_2O pressure up to 200ºC", Cem. Conc. Res. 33 271–279 (2003).

19 S.-Y. Hong, F. P. Glasser, "Phase Relations in the CaO–SiO2–H2O System to 200°C at Saturated Steam Pressure". *Cem. Conc. Res*. 34[9] 1529-1534 (2004).

20 K. S. Mamedov, N. V. Belov, "Structure of Xonotlite". *Dokl. Akad. Nauk SSSR*, 104 615-618 (1955).

21 Y. Kudoh, Y. Takeuchi, "Polytypism of Xonotlite: 1 Structures of an A-1 Polytype", *Mineralogy Journal (Japan)* 9 349–373 (1979).

22 F. Liebau, "Bemerkungen zur Systematik der Kristallstrukturen von Silikaten mit hochkondensierten Anionen". *Physikal. Chem.*, 206 73-92 (1956).

23 H. F. W. Taylor, pp. 369-370, Cement Chemistry, Academic Press, London, (1990).

24 K. Garbev, "Struktur, Eigenschaften und quantitative Rietveldanalyse von hydrothermal kristallierten Calciumsilikathydraten (C-S-H-Phasen)" (Structure, Properties and Quantitative rietveld Analysis of Hydrothermal Crystallized Calcium Silicate Hydrates (C-S-H Phases)). *PhD Thesis* Ruprecht-Karls-Universität Heidelberg, Germany, (2003).

25 K. Luke, H. F. W. Taylor, G. L. Kalousek, "Some Factors Affecting Formation of Truscottite and Xonotlite at 300–350°C". *Cem. Concr. Res*., 11[2] 197-203 (1981).

26 L. S. Dent, H. F. W. Taylor, "The Dehydration of Xonotlite". *Acta Cryst*., 9 1002-1004 (1956).

27 F. Saito, G. Mi, M. Hanada, "Mechanochemical Synthesis of Hydrated Calcium Silicates by Room Temperature Grinding". *Solid State Ionics*, 101-103 37-43 (1997).

28 H. Zur Strassen, W. Strätling, "Die Reaktion zwischen gebranntem Kaolin und Kalk in wäßriger Lösung. II. Die Reaktionsprodukte im Zusammenhang mit dem System Kalk-Kieselsäure-Tonerde-Wasser", *Zeit. Anorg. Allg. Chemie*, 245 267-278 (1940).

29 H. F. W. Taylor, "Hydrated Calcium Silicates, Part I. Compound Formation at Ordinary Temperatures", *J. Chem. Soc.*, 276 3682-3690 (1950).

30 L. Black, A. Stumm, K. Garbev, P. Stemmermann, K. R. Hallam, G. C. Allen, "X-ray Photoelectron Analysis of Cement Clinker Phases", *Cem. Concr. Res.*, 33(10) 1561-1565 (2003).

31 L. Black, K. Garbev, P. Stemmermann, K. R. Hallam, G. C. Allen, "Characterisation of Crystalline C-S-H Phases by X-ray Photoelectron Spectroscopy (XPS)", *Cem. Concr. Res*., 33[6] 899-911 (2003).

32 L. Black, K. Garbev, P. Stemmermann, K. R. Hallam, G. C. Allen "Erratum to "Characterisation of Crystalline C-S-H Phases by X-ray Photoelectron Spectroscopy (XPS),

Cement & Concrete Research, vol 33(6), (2003), pp.899-911"", *Cem. Concr. Res.*, 33[11] 1913 (2003).

33 L. Black, K. Garbev, P. Stemmermann, K. R. Hallam, G. C. Allen, "X-ray Photoelectron Study of Oxygen Bonding in Crystalline C-S-H Phases", *Phys. Chem. Minerals*, 31 337-346 (2004).

34 L. Black, K. Garbev, G. Beuchle, P. Stemmermann, D. Schild, "X-ray Photoelectron Spectroscopic Investigation of Nanocrystalline Calcium Silicate Hydrates Synthesised by Reactive Milling", *Cem. Concr. Res.*, 36 1023–1031 (2006) doi:10.1016/j.cemconres.2006.03.018.

35 M. Regourd, J. H. Thomassin, P. Baillif, J. C. Touray, "Study of the Early Hydration of Ca_3SiO_5 by X-ray Photoelectron Spectrometry", *Cem. Concr. Res.* 10 223-230 (1980).

36 J. H. Thomassin, M. Regourd, P. Baillif, J. C. Touray, "Étude de l'hydratation initiale du silicate bicalcique β par spectrométrie de photo-électrons", *C R Acad Sc Paris*, 290(Jan) 1-3 (1980).

37 H. G. M^{c}Whinney, D. L. Cocke, K. Balke, J. D. Ortego, "An Investigation of Mercury Solidification and Stabilization in Portland Cement Using X-ray Photoelectron Spectroscopy and Energy Dispersive Spectroscopy", *Cem. Concr. Res*., 20 79-91 (1990).

38 M. Y. A. Mollah, T. R. Hess, Y.-N. Tsai, D. L. Cocke, "An FTIR and XPS Investigations of the Effects of Carbonation on the Solidification/Stabilization of Cement Based Systems – Portland Type V with Zinc", *Cem. Concr. Res.*, 23 773-784 (1993).

39 K. Garbev, P. Stemmermann, L. Black, C. Breen, J. Yarwood, B. Gasharova, *J. Am. Ceram. Soc.*, 90(3), (2007), 900-907.

40 H. Seyama, M. Soma, "Bonding-state Characterization of the Constituent Elements of Silicate Minerals by X-ray Photoelectron Spectroscopy", *J Chem Soc Faraday T*, 81 485-495 (1985).

41 K. Okada, Y. Kameshima, A. Yasumori, "Chemical Shifts of Silicon X-ray Photoelectron Spectra by Polymerization Structures of Silicates", *J Am Ceram Soc*, 81[7] 1970-1972 (1998).

42 J. Chen, J. Lian, L. M. Wang, R. C. Ewing, L. A. Boater, "X-ray Photoelectron Spectroscopy Study of Irradiation-Induced Amorphization of $Gd_2Ti_2O_7$". *App. Phys. Lett.*, 79[13] 1989-1991 (2001).

43 H. Seyama, M. Soma, A. Tanaka, Surface Characterization of Acid Leached Olivines by X-Ray Photoelectron Spectroscopy, *Chem. Geol*. 129 (1996) 209–216.

44 A. Mekki, M. Salim, "XPS Study of Transition Metal Doped Silicate Glasses". *J Electron Spectrosc*, 101-103 (1999)227-232.

45 L. Black, K. Garbev, P. Stemmermann, K. R. Hallam, G. C. Allen "Simulated Degradation of a Crystalline C-S-H Phases, (Xonotlite), by X-ray Photoelectron Spectroscopy (XPS), X-ray Diffraction (XRD) and Environmental Scanning Electron Microscopy (ESEM)" *Berichte der Deutsche Mineralogischen Gesellschaft, Beih. Z. Eur. J. Mineral*. 14 (1) (2002) 21.